Supplement of Earth Surf. Dynam., 12, 581–599, 2024
https://doi.org/10.5194/esurf-12-581-2024-supplement

Earth Surface Dynamics
Open Access
EGU

Supplement of

Riverine sediment response to deforestation in the Amazon basin

Anuska Narayanan et al.

Correspondence to: Anuska Narayanan (anuska.narayanan@ufl.edu)

S1. Supplemental Information for Remote Sensing of Sediment

S1.1 Image Analysis:

Image and analysis and SSC ML algorithm development use the same methods as presented in Gardner et al., (2021) and Gardner et al., (2023). To summarize here, extraction of surface reflectance (Rs) was automated using Google Earth Engine via its python (v3.7.3) API (ee package v1.7.9), accounting for fluctuating river position, size, topographic shadows, clouds, cloud shadow, snow, ice, and river obstructions to extract only high-quality open water river channel pixels. The dynamic surface water extent (DSWE) algorithm (Jones, 2015; 2019) was used to identify high quality open water pixels in each image (See S1). Only high confidence water pixels were selected for analysis (DSWE = 1) while all other water pixels identified as water by DSWE were removed including low confidence open water (DSWE = 2), high confidence vegetated water (DSWE= 3), and low confidence vegetated water (DSWE = 4). The Landsat quality assessment band generated by FMask was used to mask clouds, cloud shadow, snow, and ice (Foga et al., 2017; Zhu et al., 2015). The global Multi-Error-Removed Improved-Terrain (MERIT) DEM (Yamazaki et al., 2017) combined with Landsat image metadata on time, location, and solar zenith was used to calculate topographic shadow using the hillshadow GEE function to mask out shaded pixels. A cumulative cost algorithm then finds connected high confidence open water pixels connected to river centerlines to identify river channel water pixels. The remaining open water river channel pixels that are not removed by the aforementioned masking procedures are used to calculate the median surface reflectance for each band across all pixels within a SWORD river reach. We applied the same procedure to extract Rs over field measurement sites to generate matchups. Matchups must occur within a +/- 1 day difference between field and satellite measurements and the median surface reflectance values were calculated for high confidence water pixels within a 500-meter buffer from the field sampling coordinates. Quality control steps include removing any match-up or reach level pixel aggregates that had less than 5 remote high confidence water pixels to remove observations impacted by neighboring non-water pixels. Matchups were also manually inspected to remove field sampling sites with coordinates that to not correspond to Landsat visible rivers and field measurements > 7500 mg/L. To account for differences in band centers and ranges of different Landsat sensors, we corrected Rs from Landsat 5 and 8 to match Landsat 7 following Gardner et al. (2021) and (Topp et al., 2021).

S1.2 SSC machine learning algorithm:

To provide representative data for training, testing, and validation, matchups were stratified into groups with approximately equal amounts of data based on SSC magnitude, site coordinates, and day of year. Within each unique combination of SSC magnitude, spatial group, and temporal group, 90% of the match-ups were randomly selected for training and validation (n=985) and the remaining 10% (n=109) were set aside as test hold-outs that are never used in training. The number of bins (4), also used as spatial-temporal cross validation folds, were chosen to balance an adequate amount of training data within each group while having groups

that capture spatial and temporal variability in SSC across the US. XGBoost was chosen because it outperformed other ML algorithms in remote sensing applications (Cao et al., 2022; Fan et al., 2020; Georganos et al., 2018) and was used in a related study using a similar approach with USGS Landsat T1-SR (Gardner et al., 2023; Topp et al., 2021). LLLTO-CV is critical for models that make spatial predictions by cross-validating the model on locations and times that were not used for model training to reduce overfitting and spatial-temporal bias (Meyer et al., 2018; Meyer et al., 2019). FFS reduces overfitting by building models with all combinations of input features while penalizing complexity to find the optimal, minimum number of features. We input Landsat's six common optical bands and 55 different spectral indices used in remote sensing of water quality for a total of 61 potential features. FFS chose 8 optimal bands/band combinations to predict SSC (Figure S2). The final model was trained using these 8 band combinations and tuned over all combinations of the four hyperparameters using a grid search to find the optimal parameter combination and model.

S1.3 Limitations:

Our remote sensing approach has limitations including use of land-based atmospheric corrections, adjacency effects, sunglint, and bottom reflectance (Mouw et al., 2015; Zheng and DiGiacomo, 2017). The Landsat 8 Surface Reflectance Correction (LaSRC) atmospheric correction algorithm performs as well as aquatic-based correction algorithms (e.g. SeaDAS, ACOLITE) for water quality applications (Kuhn et al., 2019). Many studies have successfully retrieved water quality observations from USGS T1-SR over regional to global extents using data-driven approaches (Dethier et al., 2020; Dethier et al., 2022; Olmanson et al., 2020; Topp et al., 2021). Adjacency effects in Landsat may be less severe over narrower waters such as rivers (Pahlevan et al., 2018). Sunglint may impact a small fraction of images and is minimized by calculating median reflectance values over reaches. Bottom reflectance may impact Rs, but likely only in clear rivers without vegetation since we remove vegetated water pixels using DSWE (Jones, 2015; Jones, 2019). In Gardner et al., (2021), we evaluated the potential impacts of adjacency and bottom effects by repeating trend analyses in river color for all rivers vs. rivers > 120 m, assuming the widest rivers would be deep and/or turbid enough that bottom reflectance would be minimized and found no changes in trends in river color based on river size. There are further limitations for general users of the RivSed-Amazon database. Our SSC observations only represent concentration near the surface. In very turbid rivers, our observations may only integrate over centimeters of the water column and therefore typically represent the concentration of fine sediments. Our goal was to make a coherent, basin-wide SSC database that is temporally or spatially consistent for scientific analysis. While we strive for accuracy, any given SSC observation might not be locally accurate enough for decision making that requires exact SSC thresholds. Note, our satellite observations are measuring a different spatial scale than field measurements, spatially averaging SSC over reaches (median length = 10 km) of river surface area whereas field measurements represent a discrete point. RivSed-Amazon observations are designed to be comparable with each other over time and space. The SSC algorithm will underestimate SSC in the high range (> 2,000 mg/L). We are working to resolve these issues and produce future versions of our SSC model and database that will be updated to Landsat collection 2 and include Landsat 9.

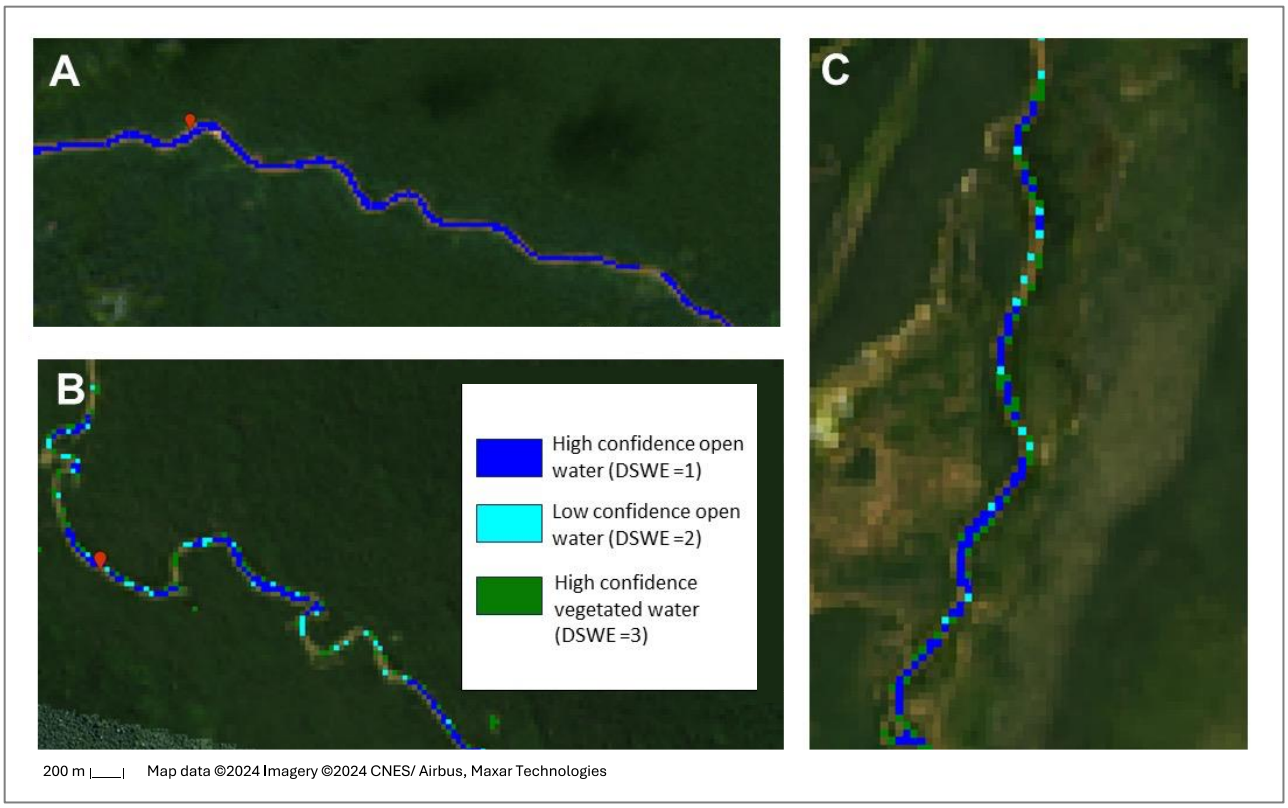

Figure S1. Examples of DSWE algorithm applied to Landsat images in three rivers in the Amazon basin that are at the edge of detection due to river widths of 30-50 meters. A) Small tributary to the Maranon River. Only DSWE =1 is shown to illustrate the selection of high-quality open water pixels only along the center of the channel (Landsat ID: LC08_L1TP_008063_20150629_20170407_01_T1). B) Rio Bacaja (Landsat ID: LC08_L1TP_225063_20150629_20170407_01_T1). C) Culuene River (Landsat ID: LC08_L1TP_225070_20150309_20170412_01_T1). Images B and C show low confidence open water and high confidence vegetated water which we exclude from analysis and are often located along the banks and sand bars. Note, any pixels not connected to the main river channel are also excluded from analysis in image processing.

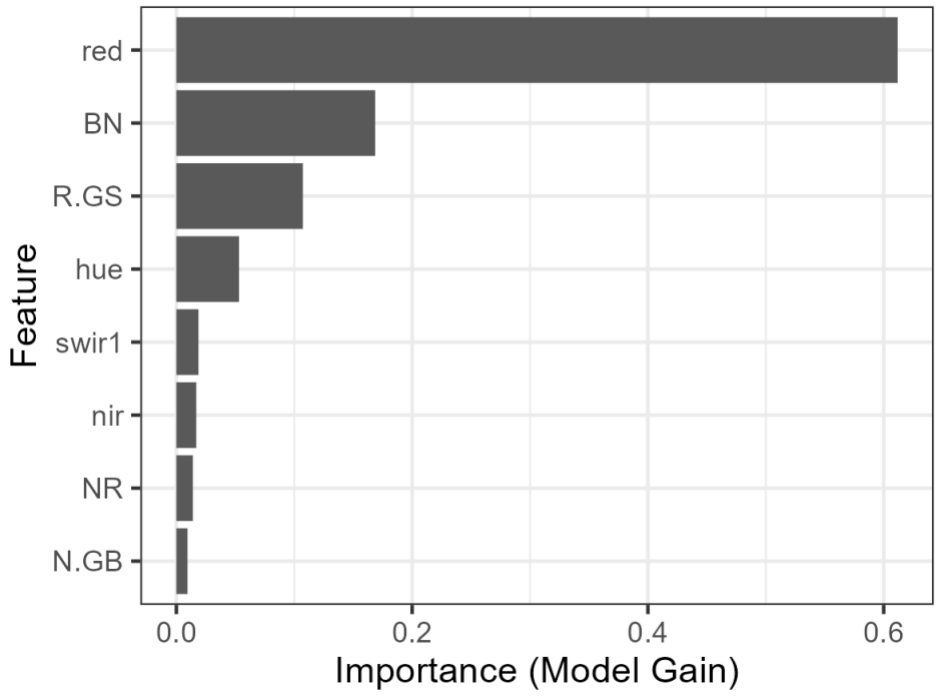

Figure S2. Feature Importance of the bands and spectral indices used in the final XGBoost regression algorithm for predicting SSC. These bands were chosen by forward-feature selection. red=red band; BN = blue/nir; R.GS = red/(green + swir1); hue = hue from the hsv colorspace calculated using rgb2hsv() function in R using the red, green, and blue bands; swir1= shortwave infrared 1; nir = near infrared; NR = nir/red; N.GB = nir/ (green +blue)

S2. Supplemental Figures of fine scale SSC trend and lag analyses

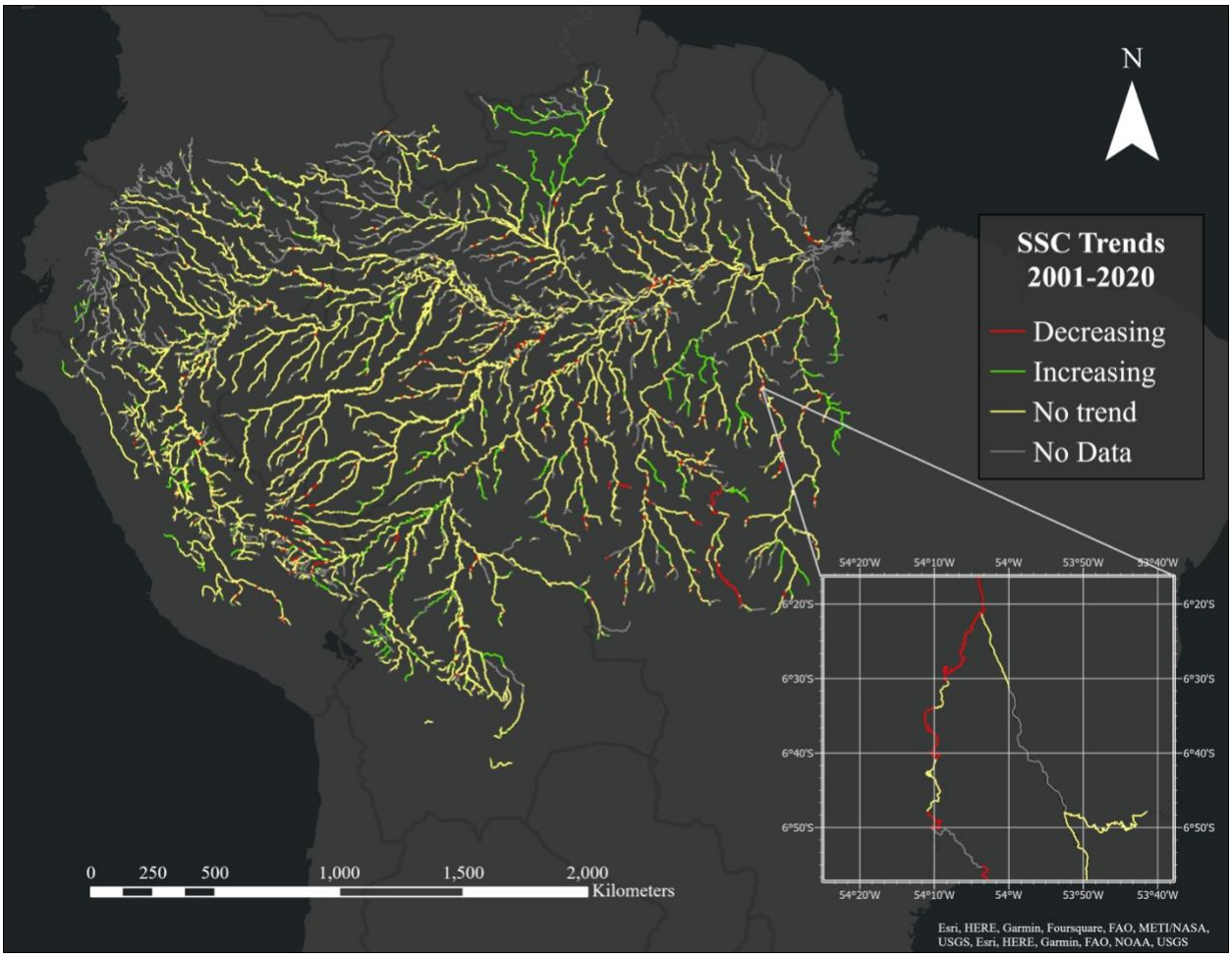

Figure S3. Reach level SSC trends for 2001-2020. Trends were calculated using a Mann-Kendall test on the median SSC recording for each year. The inset map shown in the bottom right of the figure provides an example of the heterogeneous trends observed at the river reach scale.

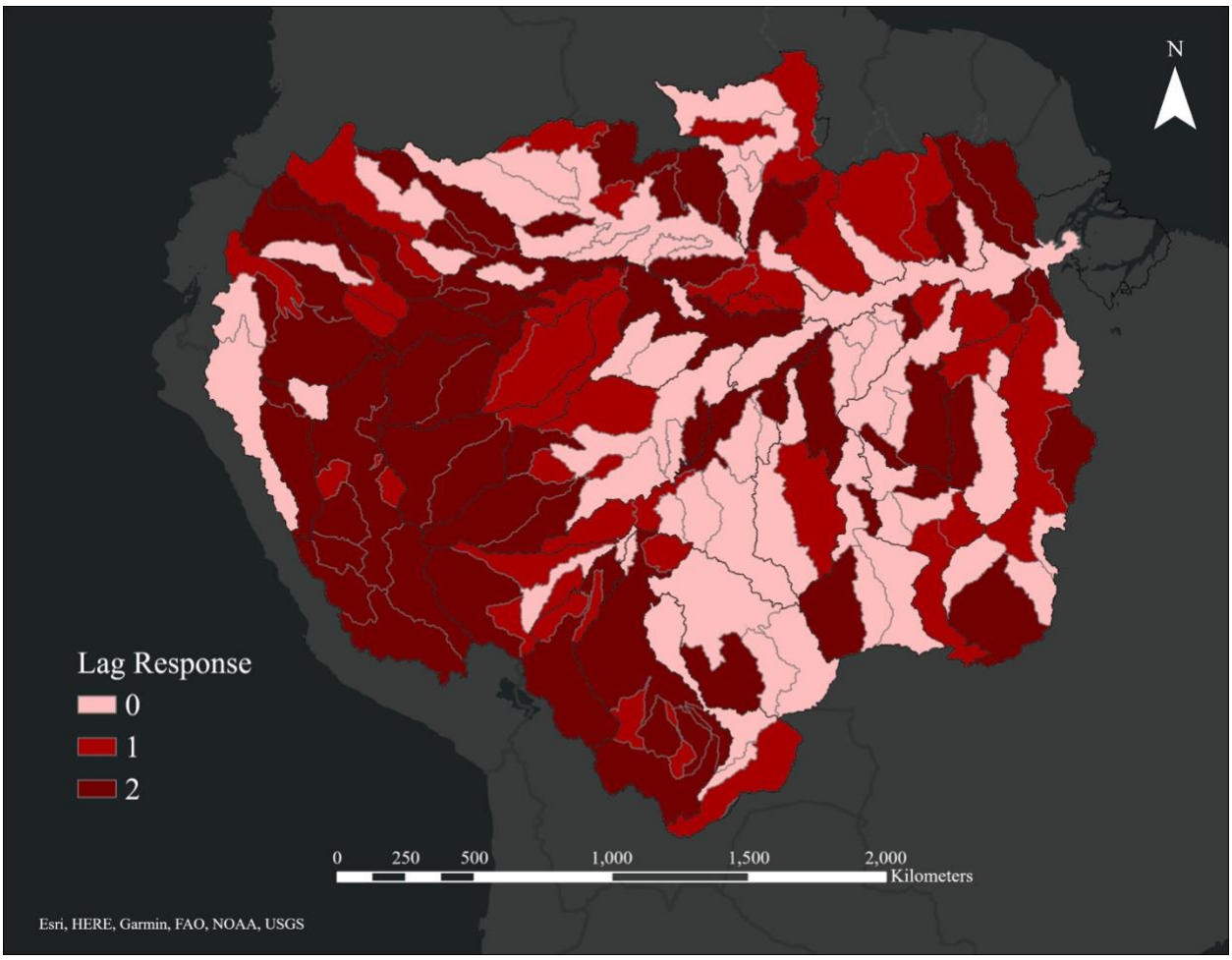

Figure S4. Lag Responses by year found in Amazonian minor tributary basins (2001-2020). Major tributary basins containing their respective minor tributary basins are delineated in black.

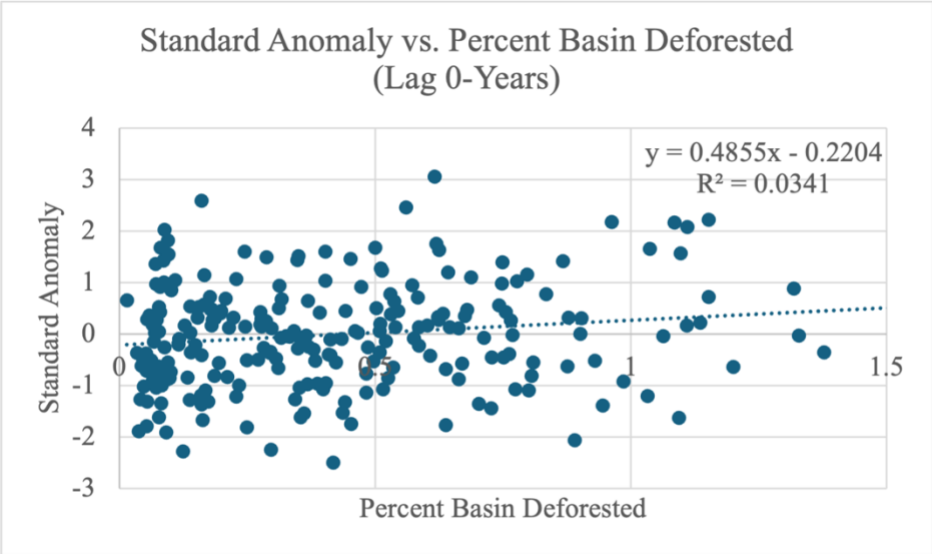

Figure S5. L0 SSC Standard Anomalies vs. Percent Basin Deforested

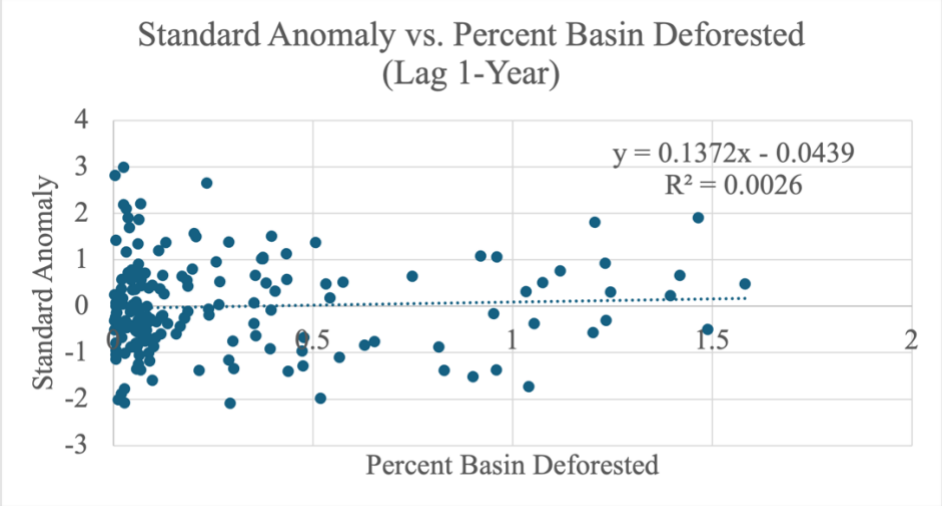

Figure S6. L1 SSC Standard Anomalies vs. Percent Basin Deforested

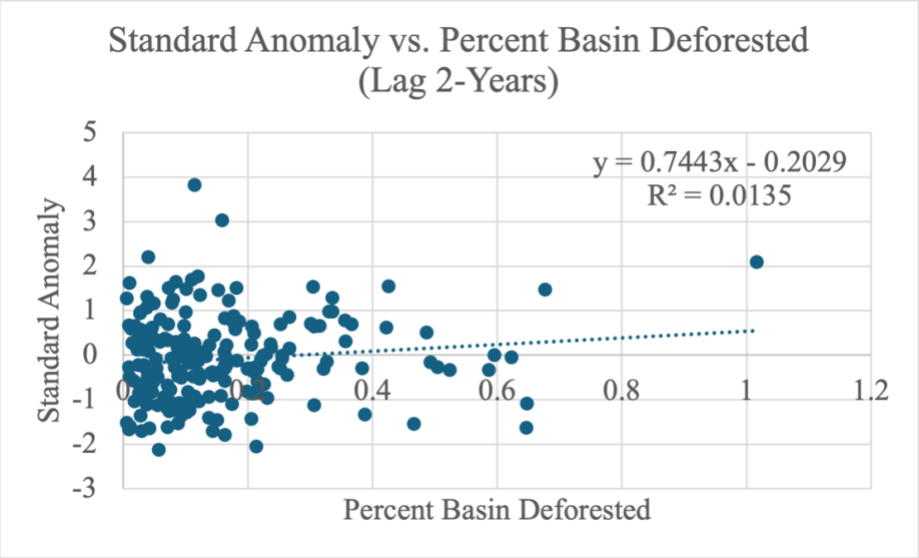

Figure S7. L2 SSC Standard Anomalies vs. Percent Basin Deforested

Supplemental References:

Altenau, E. H., Pavelsky, T. M., Durand, M. T., Yang, X., Frasson, R. P. d. M., and Bendezu, L.: The Surface Water and Ocean Topography (SWOT) Mission River Database (SWORD): A global river network for satellite data products, 57, Water Resour. Res., https://doi.org/10.1029/2021WR030054, 2021.

Cao, J., Wang, H., Li, J., Tian, Q., and Niyogi, D.: Improving the forecasting of winter wheat yields in Northern China with machine learning–dynamical hybrid subseasonal-to-seasonal ensemble prediction, Remote Sens., 14, 1707, https://doi.org/10.3390/rs14071707, 2022.

Dethier, E. N., Renshaw, C. E. and Magilligan, F. J.: Toward Improved Accuracy of Remote Sensing Approaches for Quantifying Suspended Sediment: Implications for Suspended-Sediment Monitoring, J. Geophys. Res. Earth Surf., 125, 7, https://doi.org/10.1029/2019jf005033, 2020.

Dethier, E. N., Renshaw, C. E. and Magilligan, F. J.: Rapid changes to global river suspended sediment flux by humans, Science, 376, 1447–1452, https://doi.org/10.1126/science.abn7980, 2022.

Fan, Z., Zhan, Q., Yang, C., Liu, H. and Bilal, M.: Estimating PM2.5 Concentrations Using Spatially Local Xgboost Based on Full-Covered SARA AOD at the Urban Scale, Remote Sens., 12, 3368, https://doi.org/10.3390/rs12203368, 2020.

Foga, S., Scaramuzza, P. L., Guo, S., Zhu, Z., Dilley, R. D., Jr, Beckmann, T., Schmidt, G. L., Dwyer, J. L., Joseph Hughes, M. and Laue, B.: Cloud detection algorithm comparison and validation for operational Landsat data products, Remote Sens. Environ., 194, 379–390, https://doi.org/10.1016/j.rse.2017.03.026, 2017.

Gardner, J. R., Yang, X., Topp, S. N., Ross, M. R. V., Altenau, E. H., and Pavelsky, T. M.: The Color of Rivers, Geophys. Res. Lett., 48, https://doi.org/10.1029/2020gl088946, 2021.

Gardner, J., Pavelsky, T., Topp, S., Yang, X., Ross, M. R. V., and Cohen, S. Human activities change suspended sediment concentration along rivers, Environ. Res. Lett., 18, 064032, https://doi.org/10.1088/1748-9326/acd8d8, 2023.

Georganos, S., Grippa, T., Vanhuysse, S., Lennert, M., Shimoni, M. and Wolff, E.: Very High Resolution Object-Based Land Use–Land Cover Urban Classification Using Extreme Gradient Boosting, IEEE Geosci. Remote Sens. Lett., 15, 607–611, https://doi.org/10.1109/lgrs.2018.2803259, 2018.

Jones, J.: Efficient Wetland Surface Water Detection and Monitoring via Landsat: Comparison with in situ Data from the Everglades Depth Estimation Network, Remote Sens., 7, 12503–12538, https://doi.org/10.3390/rs70912503, 2015.

Jones, J.: Improved Automated Detection of Subpixel-Scale Inundation—Revised Dynamic Surface Water Extent (DSWE) Partial Surface Water Tests, Remote Sens., 11, 374, https://doi.org/10.3390/rs11040374, 2019.

Kloiber, S. M., Brezonik, P. L., Olmanson, L. G. and Bauer, M. E.: A procedure for regional lake water clarity assessment using Landsat multispectral data, Remote Sens. Environ., 82, 38–47, https://doi.org/10.1016/s0034-4257(02)00022-6, 2002.

Kuhn, C., de Matos Valerio, A., Ward, N., Loken, L., Sawakuchi, H. O., Kampel, M., Richey, J., Stadler, P., Crawford, J., Striegl, R., Vermote, E., Pahlevan, N. and Butman, D.: Performance of Landsat-8 and Sentinel-2 surface reflectance products for river remote sensing retrievals of chlorophyll-a and turbidity, Remote Sens. Environ., 224, 104–118, https://doi.org/10.1016/j.rse.2019.01.023, 2019.

Meyer, H., Reudenbach, C., Hengl, T., Katurji, M. and Nauss, T.: Improving performance of spatio-temporal machine learning models using forward feature selection and target-oriented validation, Environ. Model. Softw., 101, 1-9, https://doi.org/10.1016/j.envsoft.2017.12.001, 2018.

Meyer, H., Reudenbach, C., Wöllauer, S. and Nauss, T.: Importance of spatial predictor variable selection in machine learning applications – Moving from data reproduction to spatial prediction, Ecol. Model., 411, 108815, https://doi.org/10.1016/j.ecolmodel.2019.108815, 2019.

Mouw, C. B., Greb, S., Aurin, D., DiGiacomo, P. M., Lee, Z., Twardowski, M., Binding, C., Hu, C., Ma, R., Moore, T., Moses, W. and Craig, S. E.: Aquatic color radiometry remote sensing of coastal and inland waters: Challenges and recommendations for future satellite missions, Remote Sens. Environ., 160, 15–30, https://doi.org/10.1016/j.rse.2015.02.001, 2015.

Olmanson, L. G., Bauer, M. E. and Brezonik, P. L.: A 20-year Landsat water clarity census of Minnesota's 10,000 lakes, Remote Sens. Environ., 112, 4086–4097, https://doi.org/10.1016/j.rse.2007.12.013, 2008.

Olmanson, L. G., Page, B. P., Finlay, J. C., Brezonik, P. L., Bauer, M. E., Griffin, C. G. and Hozalski, R. M.: Regional measurements and spatial/temporal analysis of CDOM in 10,000+ optically variable Minnesota lakes using Landsat 8 imagery, Sci. Total Environ., 724, 138141, https://doi.org/10.1016/j.scitotenv.2020.138141, 2020.

Pahlevan, N., Balasubramanian, S., Sarkar, S. and Franz, B., Toward Long-Term Aquatic Science Products from Heritage Landsat Missions, Remote Sens., 10, 1337, https://doi.org/10.3390/rs10091337, 2018.

Topp, S. N., Pavelsky, T. M., Stanley, E. H., Yang, X., Griffin, C. G. and Ross, M. R. V.: Multi-decadal improvement in US Lake water clarity, Environ. Res. Lett., 16, 055025, https://doi.org/10.1088/1748-9326/abf002, 2021.

Zheng, G. and DiGiacomo, P. M.: Detecting phytoplankton diatom fraction based on the spectral shape of satellite-derived algal light absorption coefficient, Limnol. Oceanogr., 63, 1 https://doi.org/10.1002/lno.10725, 2017.

Yamazaki, D., Ikeshima, D., Sosa, J., Bates, P. D., Allen, G. H., & Pavelsky, T. M.: MERIT Hydro: A high-resolution global hydrography map based on latest topography dataset. Water Resources Research, 55, 6, 5053-5073, https://doi.org/10.1002/2017GL072874, 2017.

Zhu, Z., Wang, S. and Woodcock, C. E.: Improvement and expansion of the Fmask algorithm: cloud, cloud shadow, and snow detection for Landsats 4–7, 8, and Sentinel 2 images, Remote Sens. Environ., 159, 269–277, https://doi.org/10.1016/j.rse.2014.12.014, 2015.